

## Article

# Mineralization of MVT Pb-Zn Deposits in the Process of Hydrocarbon Accumulation and Destruction in the Strong Structural Deformation Area of Eastern Sichuan, South China

Zhiliang He <sup>1,2,\*</sup>, Jian Gao <sup>3,4,\*</sup>, Shuangjian Li <sup>3,4</sup> and Sheng He <sup>5</sup><sup>1</sup> China Petroleum & Chemical Corporation, Beijing 100728, China<sup>2</sup> School of Earth and Space Sciences, Peking University, Beijing 100091, China<sup>3</sup> SINOPEC Petroleum Exploration and Production Research Institute, Beijing 102206, China<sup>4</sup> SINOPEC Key Laboratory of Geology and Resources in Deep Strata, Beijing 102206, China<sup>5</sup> Key Laboratory of Tectonics and Petroleum Resources of Ministry of Education, China University of Geosciences, Wuhan 430074, China

\* Correspondence: hezhiliang@sinopec.com (Z.H.); gaojian2018.syky@sinopec.com (J.G.)

**Abstract:** The Mississippi Valley-type (MVT) Pb-Zn deposits and hydrocarbon reservoirs coexist around the margin of the eastern Sichuan basin. This study examined the fluid inclusions, Sr isotope and systematic Rb-Sr, Sm-Nd geochronology for the distinct ore and gangue minerals of four orebodies from two MVT Pb-Zn deposits in the margin of the eastern Sichuan basin, combined with the existing research foundation of oil and gas accumulation and evolution, which was designed to understand the internal relationship between oil and gas accumulation and the involvement of organic matter in metal mineralization. High-density methane, moderate temperature, and salinity inclusions were discovered in the studied MVT Pb-Zn deposits, combined with relatively higher <sup>87</sup>Sr/<sup>86</sup>Sr ratios (0.71088~0.714749), indicating that the ore-forming fluids were derived largely from the hydrocarbon associated basinal brines. Rb-Sr isochron of paragenetic sphalerites and pyrites and Sm-Nd isochron of paragenetic fluorites and calcite from the studied MVT Pb-Zn deposits define isochron ages of 144.5 Ma~138.5 Ma, and 147.6 Ma, respectively, indicating that the Late Jurassic to Early Cretaceous Yanshanian orogeny was an important metallogenic event in the margin of the eastern Sichuan basin. The close temporal and spatial relationship between the MVT mineralization and hydrocarbon accumulation and destruction in the strong structural deformation area of the margin of the eastern Sichuan basin allows us to propose a possible model in which the Yanshanian compressional tectonics drove a large-scale flow of metal- and sulfate- bearing basinal fluids passed under or through methane-bearing carbonate reservoirs, resulting in the MVT mineralization and hydrocarbon accumulation and destruction.



**Citation:** He, Z.; Gao, J.; Li, S.; He, S. Mineralization of MVT Pb-Zn Deposits in the Process of Hydrocarbon Accumulation and Destruction in the Strong Structural Deformation Area of Eastern Sichuan, South China. *Minerals* **2022**, *12*, 1281. <https://doi.org/10.3390/min12101281>

Academic Editor: Thomas Gentzis

Received: 31 August 2022

Accepted: 8 October 2022

Published: 12 October 2022

**Publisher's Note:** MDPI stays neutral with regard to jurisdictional claims in published maps and institutional affiliations.



**Copyright:** © 2022 by the authors. Licensee MDPI, Basel, Switzerland. This article is an open access article distributed under the terms and conditions of the Creative Commons Attribution (CC BY) license (<https://creativecommons.org/licenses/by/4.0/>).

**Keywords:** hydrocarbon accumulation and destruction; MVT Pb-Zn deposit; high-density methane inclusions; Rb-Sr isochron dating; Sm-Nd isochron dating; coupling of mineralization and accumulation

## 1. Introduction

Fluid activities in sedimentary basins not only have an important impact on the metal mineralization, but also plays an important role in the generation, migration and accumulation of oil and gas in the reservoir. It is widely accepted that Mississippi Valley-type (MVT) Pb-Zn deposits precipitate from basinal brines, and are often symbiotic or associated with oil and gas reservoirs [1–4]. Hydrocarbons could have either directly assisted precipitation of Pb-Zn sulphides by contributing organically bound sulphur and/or sulphur from H<sub>2</sub>S-bearing natural gas, or they acted as a reducing agent in thermochemical sulphate reduction (TSR) [1,5–10]. The internal relationship between oil and gas accumulation and the involvement of organic matter in metal mineralization has always been a hot scientific issue that has been paid attention to by geologists in recent years. Extensive research on

the internal relationship has contributed greatly to our understanding of fluid flow, metal transport and oil and gas accumulation in sedimentary basins [11–15].

The margin of the eastern Sichuan basin has favorable initial conditions for the formation of hydrocarbon reservoirs and experienced large-scale hydrocarbon accumulations due to the deposition of Ediacaran-Middle Triassic marine sediments and Late Triassic-Cenozoic continental sediments, and it is a key area for the hydrocarbon exploration of marine carbonate rocks in southern China. At the same time, MVT Pb-Zn deposits are broadly represented around the margin of the eastern Sichuan basin [16]. The district contains total Pb and Zn metal reserves of more than 20 million tonnes (Mt) at average grades of 5 wt.% Pb and 10 wt.% Zn, and is the major source of base metals in China [17,18]. Although organic matter is broadly distributed in these MVT deposits, the relationship between the hydrocarbon accumulation and destruction and the regional MVT mineralization remains unresolved. Existing studies on MVT Pb-Zn deposits or hydrocarbon accumulations in the middle and upper Yangtze region are mainly limited to studying MVT Pb-Zn deposits from the perspective of ore deposit geology and hydrocarbon accumulations from the perspective of oil and gas geology. The research on the genetic internal relationship between oil and gas accumulation and MVT Pb-Zn mineralization is poorly constrained, which greatly restricts a comprehensive understanding of the metallogenic process of the MVT Pb-Zn deposits and the process of oil and gas enrichment and preservation in the study area.

In this study, we examined the fluid inclusion, Sr isotope and systematic Rb-Sr, Sm-Nd geochronology of the distinct ore and gangue minerals of four orebodies from two MVT Pb-Zn deposits in the margin of the eastern Sichuan basin, combined with the existing research foundation of oil and gas accumulation and evolution, which was designed to: (1) determine the age of the metallogenic process of the MVT Pb-Zn deposits, and discuss the temporal relationship with hydrocarbon accumulation and destruction; (2) understand the sources of organic matter in ore-forming fluids; and (3) contribute to the understanding of the internal relationship between hydrocarbon accumulation and destruction and MVT mineralization.

## 2. Geological Background and MVT Deposits

### 2.1. Geological Background

The margin of the eastern Sichuan basin is located within western Hunan and Hubei and western Hubei—eastern Chongqing (Figure 1a–c). The NE- and NEE-trending tectonic systems in the margin of the eastern Sichuan basin were formed by the basement detachment of the Jiangnan uplift and the SE-NW-trending thrust napping [19]. Tectonic deformations progressively decrease from the western Hunan and Hubei to western Hubei—eastern Chongqing and then to eastern Sichuan [20]. The study area is composed of the tectonic belts including the Sangzhi-Shimen synclinorium, the Yidu-Hefeng anticlinorium, the Huaguoping synclinorium, the Enshi anticlinorium, the Lichuan synclinorium, the Qiyueshan anticlinorium, the Shizhu synclinorium, the Fangdoushan anticlinorium, the Wanxian synclinorium, and the Kaijiang fold belt from southeast to northwest (Figure 1c).

Since the development of the basement (Yangtze craton), this study area has been affected by the Paleozoic Caledonian-Hercynian (541–251 Ma), Triassic Indosinian (251–201 Ma), Jurassic–Cretaceous Yanshanian (201–65 Ma), and Cenozoic Himalayan (65 Ma–present) tectonic orogenies, which have controlled the tectonic evolution of the eastern Sichuan basin [21]. The Caledonian, Hercynian, Yanshanian, and Himalayan tectonic movements caused uplift and erosion, leading to the relatively complex geological evolution. The Yanshanian orogeny was an important orogenic event occurring within the Yangtze block during Late Jurassic to Cretaceous, with progressive deformation from the Jiangnan-Xuefeng mountains in the southeast to the Sichuan basin in the northwest [22,23]. The stratigraphy of the eastern Sichuan basin consists of a pre-Ediacaran basement, Ediacaran to Middle Triassic submarine sedimentary sequences, and Late Triassic to Cenozoic terrigenous sediments (Figure 2; [24]). Affected by the Yanshanian and Himalayan movement, most of the

Jurassic-Quaternary sediments were eroded with only a thin set of Jurassic strata remaining in some areas [21].

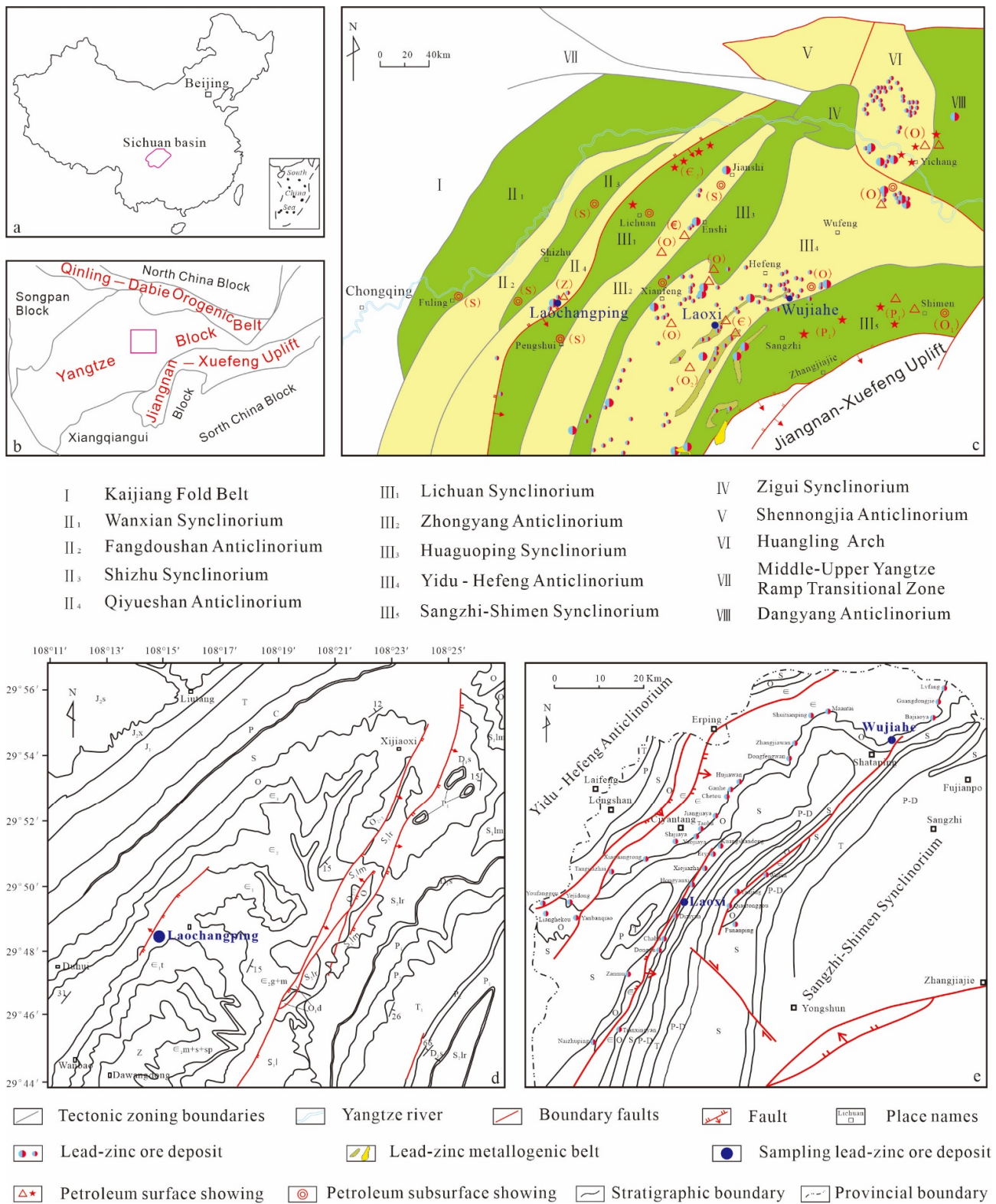


**Figure 1.** (a) Location of the Sichuan Basin in China; (b,c) simplified geological map of the margin of the eastern Sichuan, south China; (d) geologic map of the Laochangping Pb-Zn deposit; (e) geologic map of the Luota Pb-Zn deposit.

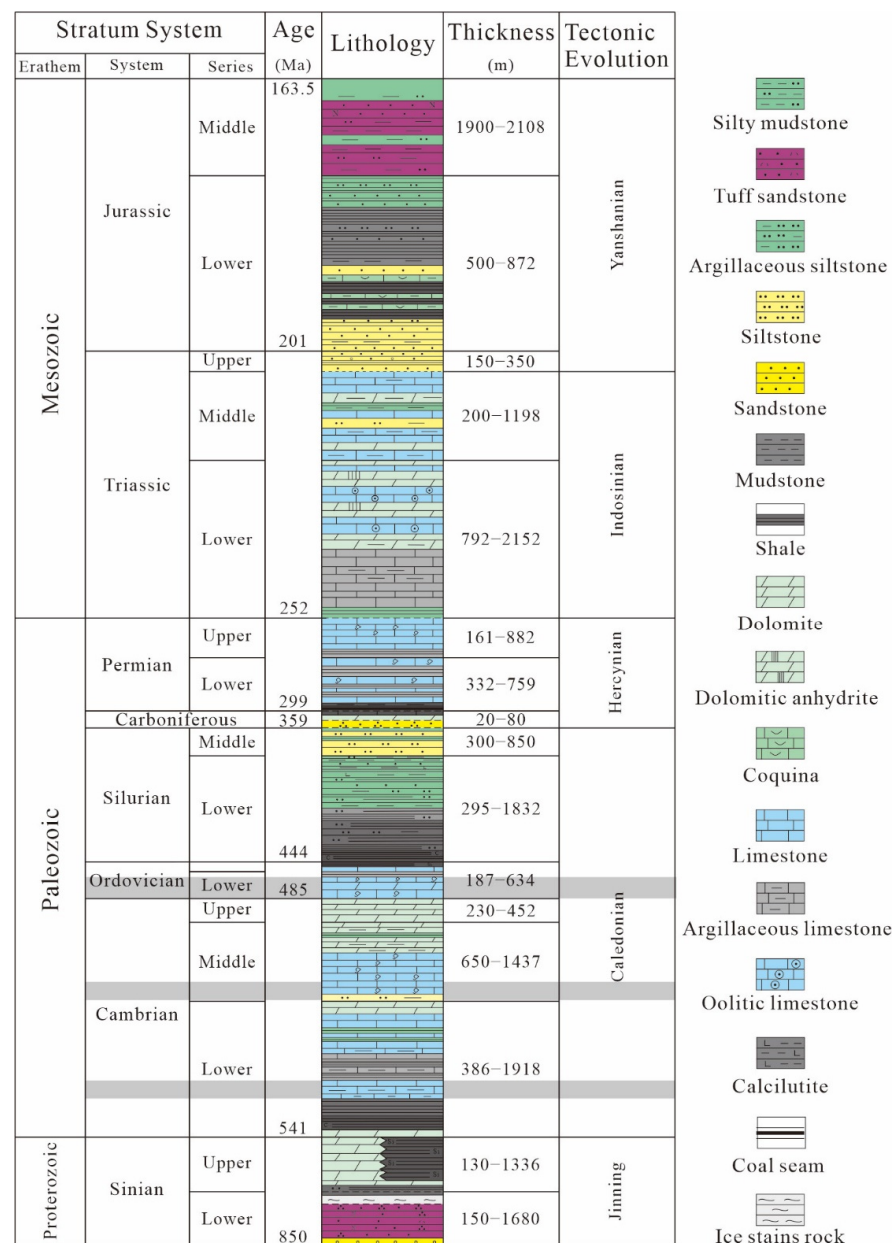


Figure 2. Schematic stratigraphic units of the margin of the eastern Sichuan basin.

### 2.2. Ore Geology

The Pb-Zn deposits within the eastern Sichuan basin are mainly hosted by carbonate rocks ranged in age from Ediacaran to Permian, and are usually located near deep-seated regional faults and spatially associated with thrust-fold systems (Figure 1c; [3,9]). The carbonate hosted Pb-Zn deposits in the eastern Sichuan basin usually formed from low-to moderate-temperature and moderate-salinity hydrothermal fluids, which have been classified as mineralization of the Mississippi Valley type [3,9,25].

The samples in this study were collected from underground exposures of the Laoxi orebody and Wujiahe orebody of the Luota Pb-Zn deposit, and the Liuhuangdong orebody and Wanbao orebody of the Laochangping Pb-Zn deposit (Figure 1d,e, Table 1). Ore textures of the two Pb-Zn deposits have been described in detail by [18,26], and only brief descriptions are provided in this paper.

**Table 1.** Details of samples selected from the Laochangping and Luota Pb-Zn deposits.

Location	Pb-Zn Mine Name	Pb-Zn Orebody Name	Latitude (°N)	Longitude (°E)	Sample	Stratigraphy	Host Lithology	Dominant Mineralogy
Shizhu synclinorium	Laochangping	Liuhuangdong	29°48'52.52"	108°15'7.80"	SH1	Lower Cambrian Qingxudong Formation	Dolomitic limestone	Sphalerite containing pyrite, galena and calcite
					SH2			Sphalerite containing pyrite and calcite
					SH3			Sphalerite containing pyrite and calcite
		Wanbao	29°54'15.91"	108°14'46.35"	WB1	Middle Cambrian Gaotai Formation	Sphalerite containing pyrite, galena and calcite	
					WB2		Pyrite containing sphalerite	
					WB3		Pyrite containing sphalerite	
Yidu-Hefeng anticlinorium	Luota	Laoxi	29°2'3.05"	109°43'38.50"	LX1	Lower Ordovician Nanjinguan Formation	Bioclastic limestone	Sphalerite containing galena and calcite
					LX2			Sphalerite containing galena and calcite
					LX3			Sphalerite containing calcite
					LX4			Sphalerite containing calcite
		Wujiahe	29°35'48.71"	110°4'29.05"	SZ1	Lower Ordovician Dawan Formation	Silicified limestone	Fluorite containing sphalerite and galena
					SZ2			Fluorite containing sphalerite
					SZ3			Fluorite containing sphalerite and galena
					SZ4			Fluorite containing sphalerite and calcite

The Laochangping Pb-Zn deposit (Figure 1d), hosted by dolomitic limestone of the Lower Cambrian Qingxudong Formation and the Middle Cambrian Gaotai Formation (Figure 2), is located in the paraxial section of the northwest flank of the Laochangping anticline in the Shizhu synclinorium. More than 80 orebodies (mineralized spots) have been discovered in this deposit, which are lenticular or layered in the interlayer fault fracture zone between NE-trending faults. The Pb-Zn orebody of this deposit is mainly produced in lenticular or layered shape, and its dip angle is between 45° and 80°, which is basically consistent with the occurrence of the strata, and the extension length along the strike is generally 50–400 m. The primary sulfide ores are mostly dense block, breccia and disseminated, and some of the ores are banded. The mineral composition is simple, the ore minerals are mainly sphalerite, galena and pyrite (Figure 3a–c), and the gangue minerals mainly include dolomite, calcite, fluorite and barite, and occasionally quartz. Sphalerite is the principal ore mineral in this deposit, mainly in light brown in color, and distributed in the ore in the form of histological clusters and dissemination.

The Luota Pb-Zn deposit is located on the southeast flank of the Yidu-Hefeng anticlinorium and the northwest flank of the Sangzhi-Shimen synclinorium on the southeastern edge of the Yangtze Platform (Figure 1e). Distribution of Pb-Zn deposit (mineralized spot) in the Luota Pb-Zn deposit is controlled by faults and fold structures, and is distributed in the core of the three anticlines. The orebodies are mainly hosted in the bioclastic limestone and silicified limestone of the Lower Ordovician Nanjinguan or Dawan Formation (Figure 2), which are mainly layered shape and veins. The layered orebodies are mostly NE-trending, with the dip southeast or northwest, dip angle ranging from 15° to 75°, extend along the strike length ranging from 50 to 3500 m, and having an average thickness of 1.33 m to 5.80 m. The ore minerals are mainly sphalerite, followed by galena and pyrite, and non-metallic minerals are mainly quartz, calcite and dolomite (Figure 3d–i).

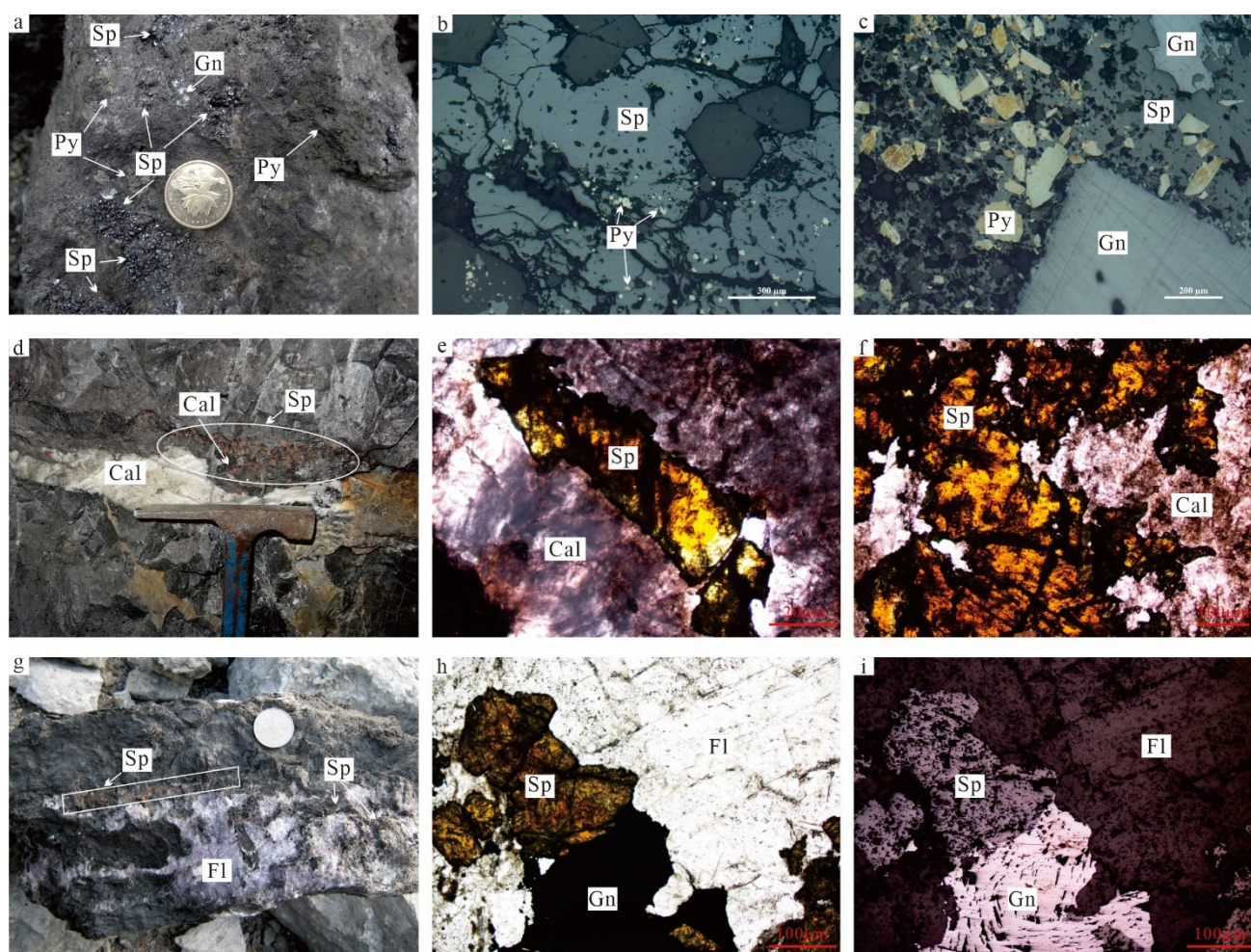


**Figure 3.** Photos of the samples showing occurrence and mineral phase characteristics of ores. (a) massive ore containing dark brown medium-fine grained sphalerite, medium-fine grained galena, and pyrite from the Laochangping Pb-Zn deposit; (b,c) sphalerite containing fine grained pyrite and galena under the reflected light microscope from the Laochangping Pb-Zn deposit; (d) underground exposure at the Laoxi orebody of the Luota Pb-Zn deposit, illustrating banded sphalerite (up) in contact with the calcite veins (down) hosted in the limestone; (e,f) light brown fine grained sphalerite coexist with calcite under the transmission light microscope from the Laoxi orebody; (g) purple fluorite coexisting with sphalerite from the Wujiahe orebody of the Luota Pb-Zn deposit; (h,i) light brown fine grained sphalerite coexisting with fine grained galena and fluorite under the microscope from the Wujiahe orebody of the Luota Pb-Zn deposit. Mineral abbreviations: Sp—sphalerite; Gn—galena; Py—pyrite; Fl—fluorite; Cal—calcite.

### 3. Methods

Hydrothermal mineral assemblage (sphalerite and pyrite) within the Liuhuangdong orebody and Wanbao orebody of Laochangping Pb-Zn deposit, and sphalerite samples within the Laoxi orebody of the Luota Pb-Zn deposit were systematically collected for Rb-Sr isochron dating and fluid inclusion analysis. Hydrothermal mineral assemblage (fluorites and calcite) within the Wujiahe orebody of the Luota Pb-Zn deposit were systematically collected for Sm-Nd isochron dating and fluid inclusion analysis (Table 1).

Sphalerite, fluorite and associated calcite samples were prepared as thin sections of approximately 30  $\mu\text{m}$  in thickness for petrographic analysis and thick doubly polished sections of approximately 100  $\mu\text{m}$  in thickness for fluid inclusion petrographic analysis, microthermometric and Raman spectral measurements. Fluid inclusion petrography and fluid inclusion assemblages were first examined using a NIKON-LV100 microscope equipped

with both transmitted white and incident ultraviolet light (UV) sources. Microthermometry of fluid inclusions was carried out using a calibrated Linkam TH-600 stage. Homogenization temperatures ( $T_h$ ) were obtained by thermal cycling [27]. Homogenization temperature measurements were determined by using a heating rate of 5 °C/min (41 °F/min). The measured temperature precisions for the homogenization temperatures is  $\pm 0.1$  °C. In this paper, we determine the paleo-fluid pressure of the metallogenic process by calculating the trapping pressures of methane inclusions. Trapping pressure was calculated following the procedures described by [28–30] according to Raman spectroscopic analyses of CH<sub>4</sub> within methane inclusions [31,32]. Raman analyses were conducted by using a JY/Horiba LabRAM HR800 Raman system with a frequency doubled Nd:YAG laser (532.06 nm). Raman spectra was collected with a laser beam being pointed at the methane inclusion to determine the CH<sub>4</sub> Raman symmetric stretching ( $\nu_1$ ) peak position. This peak position can be applied to accurately calculate the density of individual methane inclusion [32]. Trapping pressures of each methane inclusion was calculated on the basis of the density, homogenization temperature of coexisting aqueous inclusions, and equations of state for supercritical methane. Microthermometric measurements and Raman microprobe analyses have been made in the Key Laboratory of Tectonics and Petroleum Resources, China University of Geosciences in Wuhan.

Mineral separates for radiogenic isotope dating analysis were rinsed several times in distilled water, then dried and crushed to 40–60 meshes in size. The individual minerals of sphalerite, pyrite, fluorite, and calcite were handpicked under a binocular microscope, with purity levels of >99% being used for analysis. Mineral grains were washed in an ultrasonic bath and dried, then crushed to <200 meshes using an agate ball mill. Sr and Nd were separated by ion-exchange techniques, as described by [33].

Rb-Sr isotope analyses for sulfide samples were performed on a VG 354 mass spectrometer with five collectors at the Center of Modern Analysis, Nanjing University. Details of the chemical separation and mass spectrometric procedures are described by [33].  $^{87}\text{Sr}/^{86}\text{Sr}$  is normalized to  $^{86}\text{Sr}/^{88}\text{Sr} = 0.1194$ , to correct for instrumental fractionation. During the period of this study, measurements for the American Standard Reference Material NBS 987 Sr standard gave  $^{87}\text{Sr}/^{86}\text{Sr} = 0.710236 \pm 0.000007$  ( $2\sigma$ ).

Sm-Nd and  $^{87}\text{Sr}/^{86}\text{Sr}$  isotopic compositions of the fluorites and calcite analyzed during this study were also determined at the Modern Analysis Center of Nanjing University, Nanjing, China, using the procedures detailed by [33]. Analyses of the La Jolla and Standard Reference Material NBS 987 standard samples during this study yielded  $^{143}\text{Nd}/^{144}\text{Nd}$  and  $^{87}\text{Sr}/^{86}\text{Sr}$  values of  $0.511864 \pm 3$  ( $2\sigma$ ) and  $0.710236 \pm 7$  ( $2\sigma$ ), respectively. All  $^{143}\text{Nd}/^{144}\text{Nd}$  and  $^{87}\text{Sr}/^{86}\text{Sr}$  ratios determined for the samples analyzed during this study were normalized to  $^{146}\text{Nd}/^{144}\text{Nd} = 0.7219$  and  $^{86}\text{Sr}/^{88}\text{Sr} = 0.1194$ , respectively. Regression and age calculations of isochrons were performed using Isoplot/Ex Version 3.00 software, and the decay constant used in the Rb-Sr and Sm-Nd age calculation is  $\lambda^{87}\text{Rb} = 1.42 \times 10^{-11}$  year<sup>-1</sup> and  $\lambda^{147}\text{Sm} = 6.54 \times 10^{-12}$  year<sup>-1</sup>, respectively.

## 4. Results

### 4.1. Fluid Inclusions

#### 4.1.1. Fluid Inclusion Petrography

Fluid inclusions in the Laochangping Pb-Zn deposit have been conducted in sphalerites and associated calcites of the Liuhuangdong orebody. At room temperatures (25 °C), the observed primary fluid inclusion assemblages (FIAs) is mainly composed of two-phase liquid-rich inclusions (Figure 4a–c). The two-phase aqueous inclusions are ellipsoidal and amygdaloidal in shape. They contain 4 to 12 vol.% vapor and range from <5  $\mu\text{m}$  to 15  $\mu\text{m}$  in size (Figure 4). Most of the fluid inclusion assemblages in the host minerals (sphalerites and calcites) that occur as being isolated or randomly distributed within the center of the euhedral cements, and are thus considered primary fluid inclusions, possibly having been trapped during crystal growth. Secondary inclusions, present locally as trails penetrating crystal boundaries, were not used for microthermometric measurement.

Fluid inclusion analyses in the Laoxi orebody and Wujiahe orebody were carried out on sphalerites and associated calcites and fluorites. We distinguished two types of primary fluid inclusion assemblages in the main stage of mineralization at room temperature. These include two-phase aqueous inclusions and single-phase fluid inclusions. Most inclusions (up to 90%) are two-phase aqueous inclusions, and single-phase fluid inclusions are present but relatively rare. Two-phase aqueous inclusions were observed in all samples that we analysed, whereas most of the single-phase fluid inclusions were consistently observed alongside two-phase aqueous inclusions. After Raman microprobe analyses of individual fluid inclusions, part of the single-phase fluid inclusions hosted within fluorites from the Wujiahe orebody and calcites from the Laoxi orebody were found to be pure methane inclusions (Figure 4f,i). Both two-phase aqueous and single-phase fluid inclusions have irregular or rounded shape. The two-phase liquid-rich inclusions contain 5 to 10 vol.% vapor and range from  $<4\ \mu\text{m}$  to  $20\ \mu\text{m}$  in size, and the single-phase fluid inclusions are  $<8\ \mu\text{m}$  to  $25\ \mu\text{m}$  in size (Figure 4).

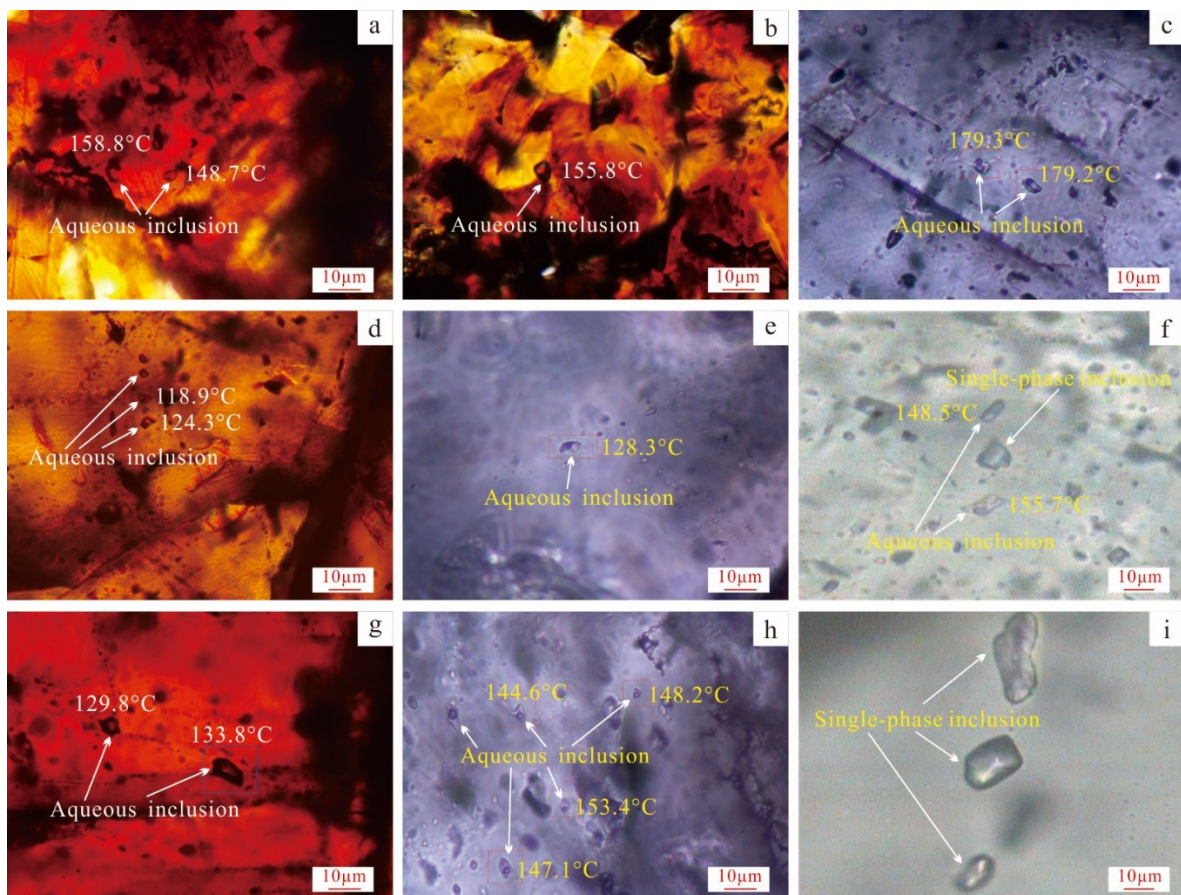


**Figure 4.** Photomicrographs under transmitted light of representative fluid inclusion types in sphalerites and associated calcites and fluorites from Liuhuangdong orebody, Laoxi orebody, and Wujiahe orebody. (a,b) representative two-phase vapour–liquid aqueous inclusions in sphalerites from Liuhuangdong orebody; (c) representative two-phase vapour–liquid aqueous inclusions in calcite from Liuhuangdong orebody; (d) representative two-phase vapour–liquid aqueous inclusions in sphalerite from Laoxi orebody; (e,f) representative two-phase vapour–liquid aqueous inclusions and single-phase inclusions in calcites from Laoxi orebody; (g) representative two-phase vapour–liquid aqueous inclusions in sphalerite from Wujiahe orebody; (h,i) representative two-phase vapour–liquid aqueous inclusions and single-phase inclusions in calcites from the Wujiahe orebody.

#### 4.1.2. Raman Spectral Analytical Results of Fluid Inclusions

Raman spectroscopy is becoming a powerful tool for quantitative analysis of fluid inclusions in geochemical environments with various temperature, pressure, and salinity [34]. After accurate calibration of Raman spectroscopic system, the Raman shift of C-H symmetric stretching ( $\nu_1$ ) band of methane can be applied to accurately calculate the density in individual fluid inclusions [29,30,32]. In this study, the 300 groove/mm grating and a spectral window of 0–4000  $\text{cm}^{-1}$  by Raman spectroscopy were adopted to check the component of the single-phase fluid inclusions. The results indicate that some analyzed single-phase fluid inclusions contain  $\text{CH}_4$  as the only detectable phase during Raman analysis. Examination of the spectral regions where the most intense peaks for  $\text{N}_2$ ,  $\text{CO}_2$  and  $\text{H}_2\text{S}$  occur failed to detect any activity (Figure 5). Those single-phase fluid inclusions are pure methane inclusions. The pure methane inclusions were studied with an 1800 groove/mm grating and a spectral window of 2750–3080  $\text{cm}^{-1}$  to measure the C-H symmetric stretching ( $\nu_1$ ) peak position of methane, calibrated with the neon lamp at room temperature (25 °C). Figure 5 gives four examples of Raman spectra of  $\text{CH}_4$  in pure methane inclusions A, B, C, and D. Methane inclusions A and B were trapped in fluorites from the Wujiahe orebody and the other two methane inclusions C and D were trapped in calcites from the Laoxi orebody. The measured  $\text{CH}_4$  symmetric stretching ( $\nu_1$ ) peak positions for pure methane inclusions A, B, C, and D correspond to a peak position of 2912.17  $\text{cm}^{-1}$ , 2912.618  $\text{cm}^{-1}$ , 2912.04  $\text{cm}^{-1}$ , and 2912.22  $\text{cm}^{-1}$ , respectively. The Raman  $\text{CH}_4$  symmetric stretching ( $\nu_1$ ) band shifts are used to calculate the density of methane inclusions according to the unified equation between  $\nu_1$  band shifts and the methane density [29,30,32], and the corresponding density for methane inclusions A, B, C, and D are 0.212  $\text{g}/\text{cm}^3$ , 0.192  $\text{g}/\text{cm}^3$ , 0.218  $\text{g}/\text{cm}^3$ , and 0.210  $\text{g}/\text{cm}^3$ , respectively. The density of methane inclusions in fluorites from the Wujiahe orebody and calcites from the Laoxi orebody is approximate, mainly ranging from 0.192  $\text{g}/\text{cm}^3$  to 0.212  $\text{g}/\text{cm}^3$ , 0.210  $\text{g}/\text{cm}^3$  to 0.218  $\text{g}/\text{cm}^3$  (Table 2), respectively. The density of methane inclusions in the studied MVT Pb-Zn deposits exceeds the critical density of methane by 0.162, and is characterized by high density.

#### 4.1.3. Fluid Inclusion Microthermometry and Trapping Pressure of Methane Inclusions

Microthermometric analyses were performed on fluid inclusions in sphalerites and associated calcites and fluorites. Most of the fluid inclusions in the sphalerites are extremely small, due to the mostly fine grained of the sphalerites. In addition, more problematic is the fact that most of the inclusions in the sphalerites appear totally dark when using normal incident light because of the strong internal reflections in the inclusion. These make it hard to study the fluid inclusions in our sphalerite samples. Even so, some microthermometric data were also measured in some relatively transparent sphalerites, which can provide the mineralization temperature of ore formation. The associated calcites and fluorites show good transparency. Measured homogenization temperatures ( $T_h$ ), final ice-melting temperatures ( $T_m$ ), and salinity data range are shown in Table 2 and Figure 6.

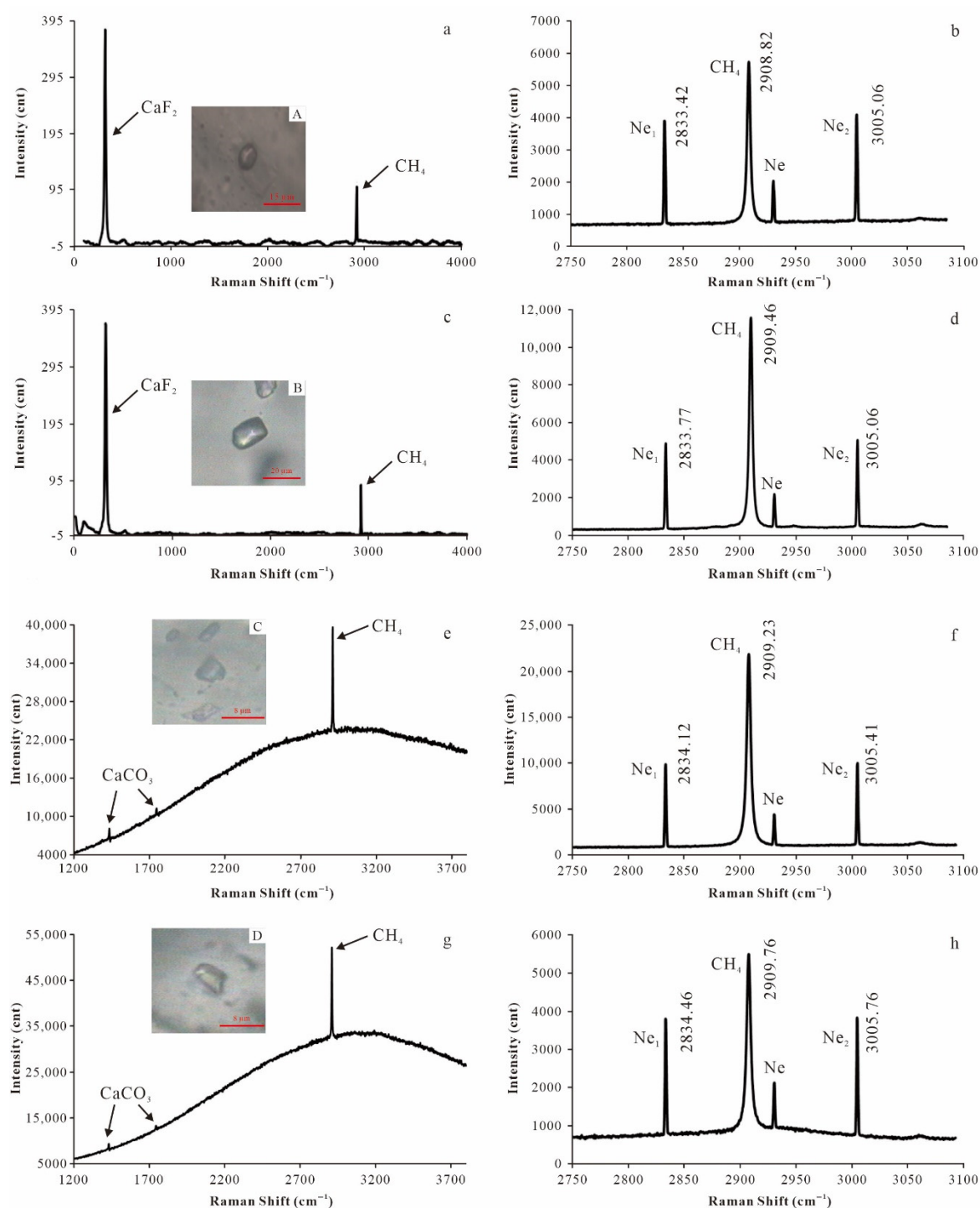


**Figure 5.** (a,c,e,g) Laser Raman spectra collected from pure methane inclusions A, B, C, and D with 300 groove/mm grating; (b,d,f,h) laser Raman spectra of CH<sub>4</sub> in pure methane inclusions A, B, C, and D with 1800 groove/mm grating. Ne<sub>1</sub> and Ne<sub>2</sub> are two bands corresponding to the Ne lamp scattering bands of 2836.99 cm<sup>-1</sup> and 3008.13 cm<sup>-1</sup>, respectively. Methane inclusions A and B were trapped in fluorites from the Wujiahe orebody, and the other two methane inclusions C and D were trapped in calcites from the Laoxi orebody.

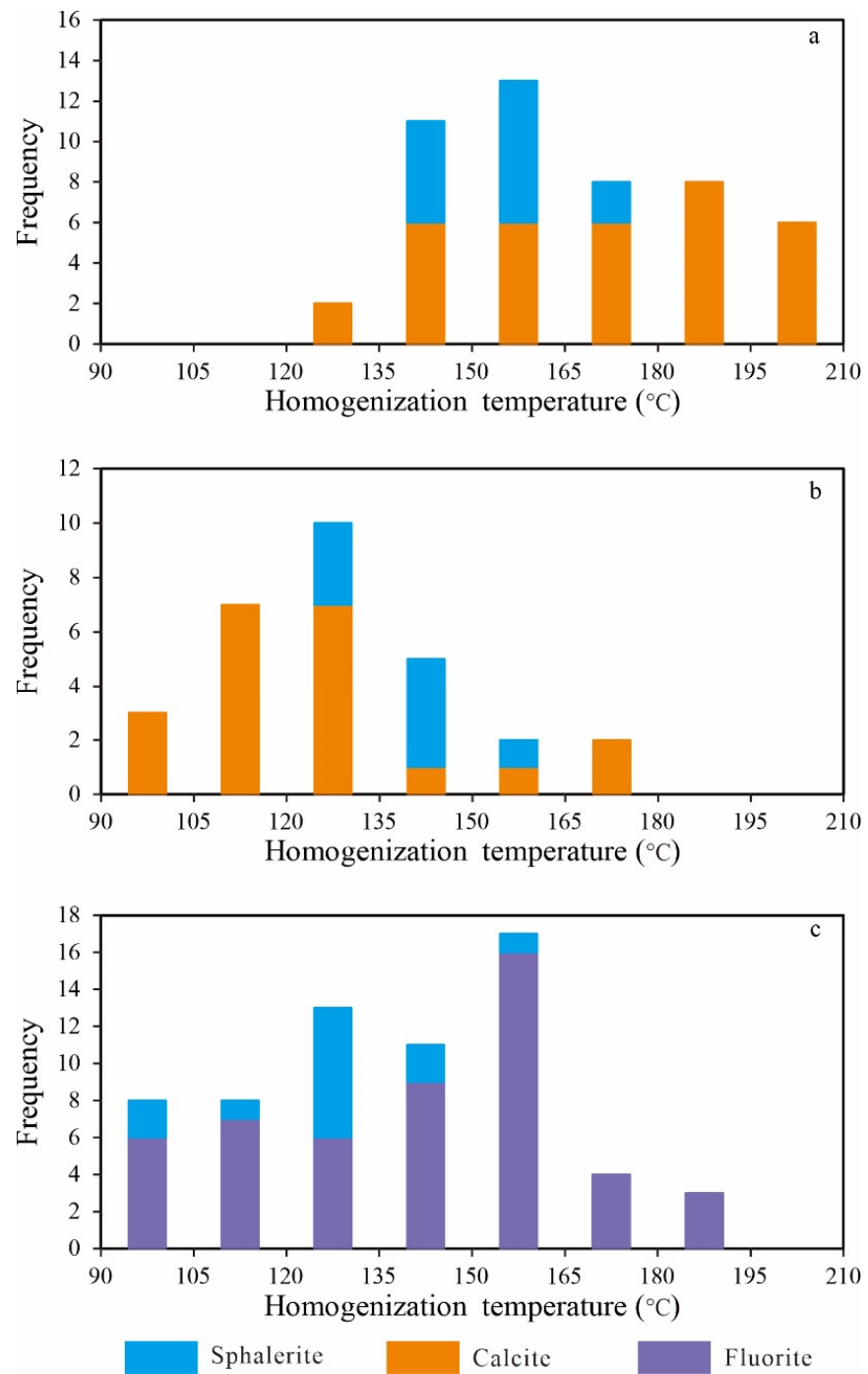


**Figure 6.** Measured homogenization temperature values of aqueous fluid inclusions of Liuhuangdong orebody (a); Laoxi orebody (b); and Wujiahe orebody (c).

**Table 2.** Measured homogenization temperatures (Th), final ice-melting temperatures (Tm) and calculated salinity data of the aqueous fluid inclusions in the Liuhuangdong orebody, Laoxi orebody, and Wujiahe orebody.

Lead–Zinc Mine Name	Lead–Zinc Orebody Name	Sample	Host Mineral	FIA	Th (Range and Mean)/(°C)		Measured Number of Aqueous Inclusion	Tm/(°C)	Salinity/(wt.% NaCl Equivalent)		
Laochangping	Liuhuangdong	SH1	Sphalerite	FIA-1	141.2–158.8	150.1	4	−11.8~−9.8 −13.4~−10.1	13.72–15.76 14.04–17.26		
				FIA-2	142.3–151.5	145.9	4				
				FIA-3	151.2–155.8	153.5	3				
				FIA-4	164.7–179.6	172.0	3				
			Calcite	FIA-1	169.4–177.4	173.4	2	−6.6~−6.1 −10.4~−7.6	9.34–9.98 11.22–14.36		
				FIA-2	179.2–192.8	185.9	4				
				FIA-3	181.2–199.5	191.1	5				
				FIA-4	182.2–200.6	193.4	4				
		SH2	Calcite	FIA-5	193.7–203.6	198.5	3	−9.6~−7.9 −12.4~−8.9	11.58–13.51 12.73–16.34		
				FIA-1	137.4–156.7	148.8	6				
				FIA-2	130.6–148.6	136.6	4				
				FIA-3	140.0–152.9	145.9	4				
		Luota	Laoxi	LX2	Sphalerite	FIA-4	166.5–176.2	171.4	2	−12.4 −17.0~−14.9 −16.4 −16.9~−9.6	16.34 18.55–20.22 19.76 13.51–20.15
						FIA-1	97.7–126.3	107.7	4		
FIA-2	100.2–124.3					114.5	3				
FIA-3	112.6–123.9					117.0	4				
FIA-4	114.0–129.8					120.6	3				
FIA-5	131.1–133.3					132.5	3				
FIA-6	142.5–155.5					149.0	2				
Calcite	FIA-7			168.8–177.8	173.3	2	−17.8~−14.1	17.87–20.82			
	FIA-1			128.3–135.9	131.5	4					
Luota	Wujiahe			SZ2	Fluorite	FIA-2	140.6–155.9	147.4	4	−12.1~−11.3 −7.6~−4.6	15.27–16.05 7.31–11.22
						FIA-1	108.2	108.2	1		
						FIA-2	137.5–143.2	139.8	3		
						FIA-3	158.5–173.9	163.5	5		
				SZ3	Sphalerite	FIA-4	181.7–192.4	187.1	2	−18.6 −16.4~−21.5	21.4 19.76–23.37
		FIA-1	101.2–117.3			109.3	2				
		FIA-2	121.4–134.6			127.9	4				
		FIA-3	127.6–134.8		130.7	3					
		FIA-4	144.2–161.6		151.3	3					
		Fluorite	FIA-1		93.2–106.5	98.8	3	−12.1~−10.9	14.87–16.05		
FIA-2	127.6–136.5		131.5	5							
FIA-3	144.6–153.4		148.3	4							
SZ3	Fluorite	FIA-4	153.2–158.4	156.8	4	−12.4~−11.3 −12.5	15.27–16.34 16.43				
		FIA-5	162.3	162.3	1						

Table 2. Cont.

Lead–Zinc Mine Name	Lead–Zinc Orebody Name	Sample	Host Mineral	FIA	Th (Range and Mean)/(°C)	Measured Number of Aqueous Inclusion	T <sub>m</sub> /(°C)	Salinity/(wt.% NaCl Equivalent)	
			Sphalerite	FIA-1	93.2–118.6	105.9			
				FIA-2	121.7–133.8	127.6	2	–17.6	20.67
		SZ4	Fluorite	FIA-1	93.7–106.8	101.7	3	–13.5~–8.9	12.73–17.34
				FIA-2	96.2~109.6	104.4	4	–7.7	11.34
				FIA-3	114.3–118.6	116.45	2	–15.2	18.8
				FIA-4	130.8–164.4	146.1	5	–6.1	9.34
				FIA-5	162.3–167.1	164.7	6	–12.1~–8.9	12.73–16.05
				FIA-6	174.8–188.4	181.6	2		

Microthermometric data of the Liuhuangdong orebody show that fluid inclusions in sphalerites have average Th values of 145.9–172.0 °C and Tm values of −13.4–−9.8 °C, corresponding to salinities of 13.72–17.26 wt.% NaCl equivalent. The average Th values of fluid inclusions in calcites ranges from 136.6 °C to 198.5 °C, and Tm values range from −12.4 °C to −6.1 °C, corresponding to salinities of 9.34–16.34 wt.% NaCl equivalent (salinity calculation based on [35]).

Microthermometric data of the Laoxi orebody show that the average Th values of aqueous inclusion assemblages in sphalerites varies from 107.7 °C to 173.3 °C, and Tm values vary from −17.0 °C to −9.6 °C, corresponding to salinities of 13.51–20.22 wt.% NaCl equivalent. The average Th values of fluid inclusions in calcites ranges from 131.5 °C to 147.4 °C, and Tm values range from −17.8 °C to −14.1 °C, corresponding to salinities of 17.87 to 20.82 wt.% NaCl equivalent. Fluid pressures at inclusion trapping conditions were calculated based on the density of methane inclusions, homogenization temperature of coexisting aqueous inclusions, and the equation of state (EOS) for supercritical methane by [36]. The calculated trapping pressures of methane inclusions in calcites within the Laoxi orebody mainly range from 53.5 MPa to 60.8 MPa.

Microthermometric data of the Wujiahe orebody show that fluid inclusions in sphalerites have average Th values of 105.9–151.3 °C and Tm values of −21.5–−16.4 °C, corresponding to salinities of 19.76–23.37 wt.% NaCl equivalent. The average Th values of fluid inclusions in fluorites ranges from 98.8 °C to 187.1 °C, and Tm values range from −15.2 °C to −4.6 °C, corresponding to salinities of 7.31 to 18.8 wt.% NaCl equivalent. The calculated trapping pressures of methane inclusions in fluorites within the Wujiahe orebody mainly range from 46.9 to 66.8 MPa.

#### 4.2. Rb-Sr and Sm-Nd Geochronology of the MVT Pb-Zn Deposits

##### 4.2.1. Rb-Sr Isochron Ages of the Laochangping Pb-Zn Deposits

Four sphalerite samples and two paragenetic pyrite samples, extracted from the Liuhuangdong orebody, were analyzed for Rb and Sr isotopes. Meanwhile, four pyrite samples and one paragenetic sphalerite sample within the Wanbao orebody were extracted for Rb and Sr isotopic analysis. The results of Rb and Sr concentrations and their isotopic compositions of the samples are given in Table 3 and Figure 7. Isotope dilution measurements on samples from the Liuhuangdong orebody show Rb and Sr concentrations of 0.19–0.94 ppm and 0.61–6.5 ppm, respectively. Samples from the Wanbao orebody contain 0.56–2.01 ppm Rb and 0.68–2.01 ppm Sr. Sr concentrations of pyrite samples from the Liuhuangdong orebody are generally higher than those of the Wanbao orebody. The values of  $^{87}\text{Rb}/^{86}\text{Sr}$  in the Liuhuangdong orebody and Wanbao orebody range from 0.306 to 1.341 and 1.268 to 8.397, respectively. The values of  $^{87}\text{Sr}/^{86}\text{Sr}$  in the Liuhuangdong orebody and Wanbao orebody have a relatively wide range from 0.715237 to 0.717372 and 0.714311 to 0.728832, respectively. On the  $^{87}\text{Rb}/^{86}\text{Sr}$ – $^{87}\text{Sr}/^{86}\text{Sr}$  diagrams, two groups of paragenetic mineral assemblage display a good linear relationship, respectively (Figure 7a,b), which represent an isochron or a mixed line with two end-members of different  $^{87}\text{Rb}/^{86}\text{Sr}$  and  $^{87}\text{Sr}/^{86}\text{Sr}$  ratios. Because no linear relationships exist on the  $1/\text{Sr}$ – $^{87}\text{Sr}/^{86}\text{Sr}$  diagrams for the paragenetic mineral assemblage of the Liuhuangdong orebody or the Wanbao orebody (Figure 8a,b), we can rule out the possibility of a mixed line. Analytical data of the Liuhuangdong orebody yield an isochron age of  $144.5 \pm 3.9$  Ma with an initial  $^{87}\text{Sr}/^{86}\text{Sr}$  ratio of  $0.714638 \pm 0.000051$  and the mean square of weighted deviates (MSWD) value of 0.78 (Figure 7a). The analytical data of the Wanbao orebody yield an isochron age of  $142.9 \pm 2.5$  Ma with an initial  $^{87}\text{Sr}/^{86}\text{Sr}$  ratio of  $0.71170 \pm 0.00021$  and MSWD value of 0.31 (Figure 7b).

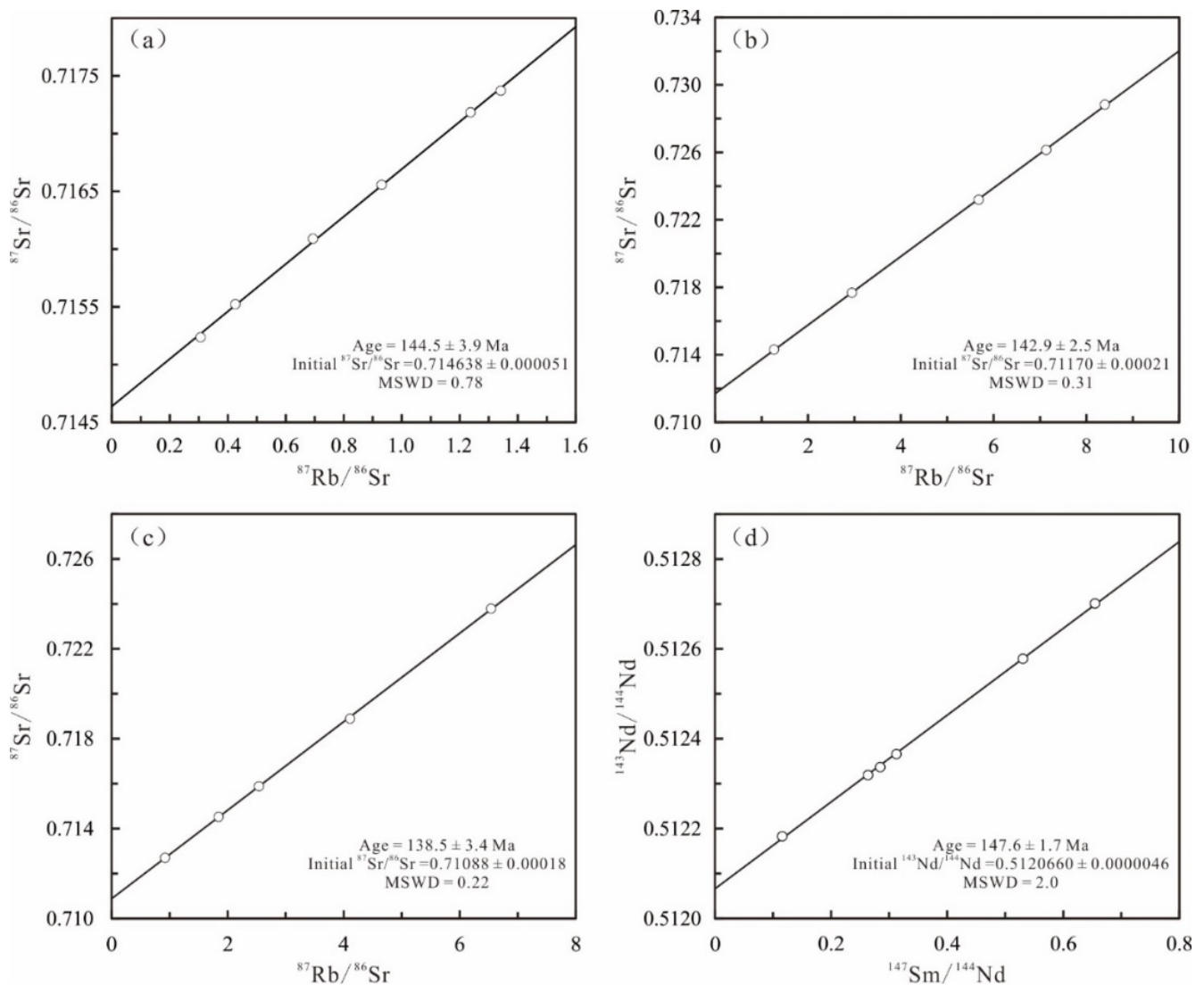


**Figure 7.** Rb-Sr and Sm-Nd isochron diagrams of the Laochangping and Luota Pb-Zn deposits. (a) Rb-Sr isochron of paragenetic sphalerites and pyrites from the Liuhuangdong orebody in the Laochangping Pb-Zn deposit; (b) Rb-Sr isochron of paragenetic sphalerite and pyrites from the Wanbao orebody in the Laochangping Pb-Zn deposit; (c) Rb-Sr isochron of sphalerites from the Laoxi orebody in the Luota Pb-Zn deposit; (d) Sm-Nd isochron of paragenetic fluorites and calcite from the Wujiahe orebody in the Luota Pb-Zn deposit.

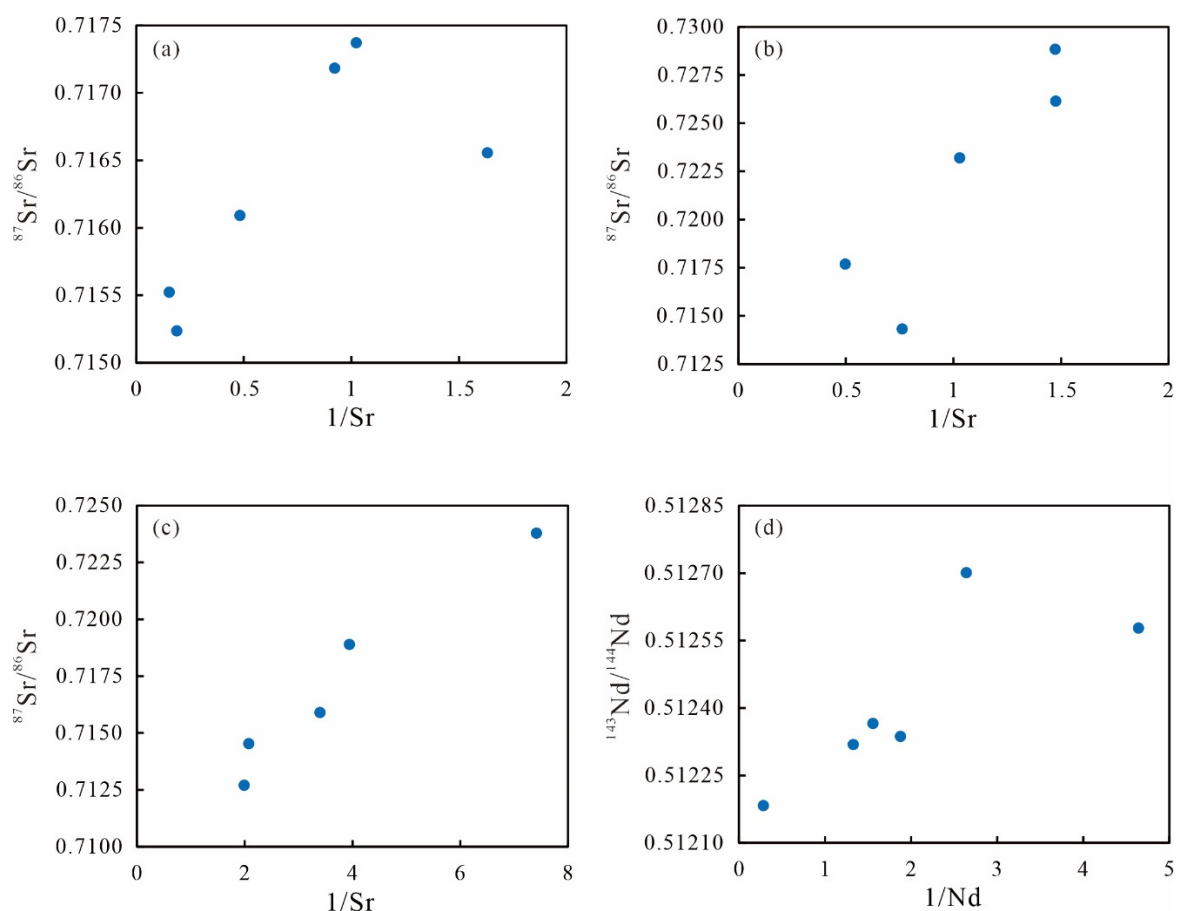


**Figure 8.**  $^{87}\text{Sr}/^{86}\text{Sr}$  vs.  $1/\text{Sr}$  diagrams for (a) paragenetic sphalerites and pyrites from the Liuhuanguandong orebody in the Laochangping Pb-Zn deposit, (b) paragenetic sphalerite and pyrites from the Wanbao orebody in the Laochangping Pb-Zn deposit and (c) sphalerites from the Laoxi orebody in the Luota Pb-Zn deposit. (d)  $^{143}\text{Nd}/^{144}\text{Nd}$  vs.  $1/\text{Nd}$  diagrams for paragenetic fluorites and calcite from the Wujiahe orebody in the Luota Pb-Zn deposit. Note that the plots show no linear relationships, ruling out the possibility of two-component mixing and suggesting that the Rb-Sr and Sm-Nd isochron ages in Figure 7 are geologically meaningful.

**Table 3.** Analytical data of Rb-Sr isotopic ratios and Rb-Sr concentrations of the sulfide samples from the Laochangping and Luota Pb-Zn deposits.

Pb-Zn Mine Name	Pb-Zn Orebody Name	Sample Number	Mineral	Rb ( $\mu\text{g/g}$ )	Sr ( $\mu\text{g/g}$ )	$^{87}\text{Rb}/^{86}\text{Sr}$	$^{87}\text{Sr}/^{86}\text{Sr}$ ( $2\sigma$ )
Laochangping	Liuhuanguandong	SH1	Sphalerite	0.4897	2.078	0.6937	$0.716091 \pm 9$
		SH1	Pyrite	0.5513	5.314	0.3061	$0.715237 \pm 12$
		SH2	Pyrite	0.9382	6.503	0.4259	$0.715523 \pm 9$
		SH2	Sphalerite	0.4451	0.9781	1.341	$0.717372 \pm 8$
		SH2	Sphalerite	0.4509	1.885	1.237	$0.717184 \pm 11$
		SH3	Sphalerite	0.1928	0.6127	0.9305	$0.716557 \pm 9$
	Wanbao	WB1	Sphalerite	0.5632	1.314	1.268	$0.714311 \pm 8$
		WB1	Pyrite	1.874	0.9725	5.679	$0.723193 \pm 9$
		WB2	Pyrite	1.931	0.6789	8.397	$0.728832 \pm 9$
WB2		Pyrite	1.639	0.6775	7.134	$0.726145 \pm 9$	
WB3		Pyrite	2.015	2.013	2.945	$0.717679 \pm 9$	
Luota	Laoxi	LX1	Sphalerite	0.1579	0.5031	0.921	$0.712701 \pm 8$
		LX2	Sphalerite	0.2381	0.4817	1.842	$0.714528 \pm 6$
		LX2	Sphalerite	0.2537	0.2946	2.537	$0.715890 \pm 10$
		LX3	Sphalerite	0.2986	0.1349	6.539	$0.723791 \pm 8$
		LX4	Sphalerite	0.3249	0.2537	4.108	$0.718894 \pm 8$

#### 4.2.2. Rb-Sr Isochron Age of the Liaoxi Orebody

The analyzed five sphalerite samples extracted from the Laoxi orebody yield Rb and Sr concentrations of 0.158–0.325 and 0.135–0.503 ppm, respectively. The five sphalerites have  $^{87}\text{Rb}/^{86}\text{Sr}$  ratios of 0.0914 to 6.539 and  $^{87}\text{Sr}/^{86}\text{Sr}$  ratios of 0.710922 to 0.723791 (Table 3). Analytical data of the Laoxi orebody yield an isochron age of  $138.5 \pm 3.4$  Ma with an initial  $^{87}\text{Sr}/^{86}\text{Sr}$  ratio of  $0.71088 \pm 0.00018$  and MSWD value of 0.22 (Figure 7c). The  $1/\text{Sr}$  values of the sphalerite samples do not covary with  $^{87}\text{Sr}/^{86}\text{Sr}$  values (Figure 8c), indicating that the isochron age is meaningful and should represent the timing of ore formation.

#### 4.2.3. Sm-Nd Isochron Age and Sr Isotopic Compositions of the Wujiahe Orebody

Five fluorites and one paragenetic calcite in the Wujiahe orebody were used for both Sm-Nd dating and Sr isotopic analysis. Abundances of Sm and Nd and its Nd and Sr isotopic compositions are listed in Table 4. The samples analyzed during this study yield Sm and Nd concentrations of 0.189–0.733 and 0.215–3.526 ppm, respectively. These samples have  $^{147}\text{Sm}/^{144}\text{Nd}$  ratios and  $^{143}\text{Nd}/^{144}\text{Nd}$  ratios of 0.1159–0.6547 and 0.512183–0.512701, respectively. The paragenetic fluorites and calcite yield an isochron slope corresponding to an age of  $147.6 \pm 1.7$  Ma and an intercept of 0.512066, with MSWD value being 2 (Figure 7d). In addition, a lack of linear relationships between the  $1/\text{Nd}$  and  $^{143}\text{Nd}/^{144}\text{Nd}$  values of these samples excludes the possibility of the mixing of different isochrons (Figure 8d), and suggests that the Sm-Nd age obtained during this study is robust. Sr isotopic analyses were also performed on the same separates. The fluorites and paragenetic calcite have homogeneous  $^{87}\text{Sr}/^{86}\text{Sr}$  compositions of between 0.713753 and 0.714749 (Table 4). Considering that fluorite and calcite are calcic minerals, who usually have a very low Rb/Sr ratio, these Sr isotopic ratios allowed us to determine the source of ore-forming fluids directly [37,38].

**Table 4.** Sm-Nd and Sr isotopic compositions of fluorites and paragenetic calcite from the Luota MVT Pb-Zn deposit.

Pb-Zn Mine Name	Pb-Zn Orebody Name	Sample Number	Mineral	Sm ( $\mu\text{g/g}$ )	Nd ( $\mu\text{g/g}$ )	$^{147}\text{Sm}/^{144}\text{Nd}$	$^{143}\text{Nd}/^{144}\text{Nd}$ ( $2\sigma$ )	$^{87}\text{Sr}/^{86}\text{Sr}$ ( $2\sigma$ )
Luota	Wujiahe	SZ1	Fluorite	0.3267	0.7521	0.2634	$0.512319 \pm 9$	$0.714058 \pm 9$
		SZ2	Fluorite	0.4092	0.3782	0.6547	$0.512701 \pm 8$	$0.714152 \pm 8$
		SZ3	Fluorite	0.3314	0.6421	0.3125	$0.512366 \pm 10$	$0.714227 \pm 7$
		SZ3	Fluorite	0.2507	0.5326	0.2846	$0.512337 \pm 9$	$0.713753 \pm 9$
		SZ4	Fluorite	0.1886	0.2154	0.5304	$0.512578 \pm 8$	$0.714749 \pm 11$
		SZ4	Calcite	0.7325	3.526	0.1159	$0.512183 \pm 10$	$0.713814 \pm 6$

## 5. Discussion

### 5.1. Possible Sources of Ore-Forming Fluids

Generally, Sr isotopes do not undergo any significant mass fractionation during most geological processes [39]. Hence, Sr isotopic signature of a fluid will reflect the Sr isotopic values of the rocks with which that fluid has equilibrated. The initial  $^{87}\text{Sr}/^{86}\text{Sr}$  ratios of the Liuhuangdong, Wanbao, and Laoxi orebodies are 0.714638, 0.714638, and 0.71088, respectively. The  $^{87}\text{Sr}/^{86}\text{Sr}$  ratios of fluorites and paragenetic calcite in the Wujiahe orebody range from 0.713753 to 0.714749. In comparison to  $^{87}\text{Sr}/^{86}\text{Sr}$  values of the Emeishan basalts or other mantle-derived fluids (0.702–0.706, [40–42]) and Lower Paleozoic marine carbonated sediments (0.7075–0.7111, [43]), the studied MVT Pb-Zn deposits have relatively higher  $^{87}\text{Sr}/^{86}\text{Sr}$  values, which essentially overlap with those of Lower Cambrian Niutitang Formation shales in the study area [44–46]. Accordingly, we infer that such higher  $^{87}\text{Sr}/^{86}\text{Sr}$  values seen in the studied MVT Pb-Zn deposits were derived largely from the Lower Cambrian Niutitang Formation sources. In addition, the Lower Cambrian Niutitang Formation shales are considered as the high-quality regional source rocks of oil and gas, suggesting that the ore-precipitating fluids could have been derived from the hydrocarbon associated brines rather than from the average basinal fluids.

The study of fluid inclusion in hydrothermal ore deposits is a useful tool to give an insight into the physico-chemical conditions during ore formation. For MVT deposits, fluid inclusion studies have contributed greatly towards a better understanding of the conditions and processes of their formation [8]. Microthermometric data show the Laochangping and Luota Pb-Zn deposits resulted from precipitation at moderate temperature (105–200 °C), from fluids with low to moderate salinity (9.3–20.8 wt.% NaCl equivalent). The temperature and salinity of ore-forming fluids we have determined are similar to those of the basinal brine. Although most models for MVT mineralization suggest sulphide precipitation through sulphate reduction by methane or other organic matter [8], the reports of the occurrence of significant amounts of methane in ore-precipitating fluids are rare. This study shows that the presence of single-phase high density methane inclusions was intimately associated with MVT mineralization. Single-phase methane inclusions alongside two-phase inclusions were observed in the associated calcites and fluorites, indicating that the ore-forming fluids were saturated with methane, and a methane phase existed as a separate immiscible fluid phase at the time of ore formed. High-density methane is often considered to be related to liquid hydrocarbon cracking gas in hydrocarbon reservoirs. Our previous studies found that a large amount of gas generated from the conversion of kerogen and liquid hydrocarbon can be the main contributor to the high-density methane and abnormally high pressure in the hydrocarbon reservoir [29,30]. Thus, together with geochemical data discussed here, it is plausible to argue that the ore-precipitating fluids could have been derived from the hydrocarbon associated brines, resulting in the relatively higher  $^{87}\text{Sr}/^{86}\text{Sr}$  ratios, moderate temperature and salinity, and the methane-saturated of ore-forming fluids.

### 5.2. Timing of MVT Pb-Zn Deposits Mineralization

The isotopic dating of ore minerals is the best method to determine the age of a MVT Pb-Zn deposit. The Rb-Sr and Sm-Nd isotopic systems are generally considered to be a closed system, and are capable of resisting isotopic resetting as a result of alteration and/or weathering to some degree. Different mineral phases have different chemical potential, which can cause the Rb-Sr and Sm-Nd with distinct chemical properties to be differentiated with different Rb/Sr values and Sm/Nd values in the paragenetic minerals precipitated from the same ore forming fluids. Therefore, it is advantageous to use hydrothermal mineral assemblage to date the formation of hydrothermal deposits [47]. In the present study, Rb-Sr isochron of paragenetic sphalerites and pyrites from the Laochangping Pb-Zn deposit, Sm-Nd isochron of paragenetic fluorites and calcite from the Wujiahe orebody in the Luota Pb-Zn deposit, and Rb-Sr isochron of sphalerites from the Laoxi orebody in the Luota Pb-Zn deposit define isochron ages of 142.9–144.5 Ma, 147.6 Ma, and 138.5 Ma, respectively, indicating that the Late Jurassic to Early Cretaceous was an important metallogenic event in the margin of the eastern Sichuan basin. The Yanshanian orogeny was an important orogenic event occurring within the Yangtze Block during the Late Jurassic to Cretaceous, with progressive deformation from the Jiangnan–Xuefeng mountains in the southeast to the Sichuan basin in the northwest [22,23]. The Rb-Sr and Sm-Nd isochron ages of the studied MVT Pb-Zn deposits agree well in timing with the main episode of the Early Yanshanian tectonic movement in the study area. Thus, we consider that metal mineralization of MVT deposits in the margin of the eastern Sichuan basin involved the large-scale migration of hydrocarbon associated basinal brines triggered by the Early Yanshanian orogenic events.

### 5.3. Implication for MVT Mineralization Model around the Margin of the Eastern Sichuan Basin

The MVT Pb-Zn deposits and hydrocarbon reservoirs coexist around the margin of the eastern Sichuan basin. In addition, the ore-forming fluids, derived largely from the hydrocarbon associated basinal brines, have been revealed in this study. It would be interesting to determine whether the hydrocarbon accumulation and destruction and MVT Pb-Zn mineralization had been broadly contemporaneous or not, and whether they were controlled by the same geodynamic events.

The vast majority of data on hydrocarbon accumulation times in the literature suggest that Lower Cambrian Niutitang Formation shales or other marine source rocks had reached the over mature stage during the Late Indosinian to Early Yanshanian (the end of the Triassic to the Early Jurassic), and the liquid hydrocarbon and wet gas generated in the low to high mature stage were thermally cracked into methane at the over mature stage. From the late stage of Middle Jurassic to Early Cretaceous, the middle-upper Yangtze, confined and controlled by the Qinling orogenic belt to the north and the Jiangnan fold-uplift belt to the southeast, has suffered multi-directional plate convergence and multiphase intense intracontinental orogeny [48]. As a result, the oil and gas in this region generally experienced modification, adjustment, re-accumulation, and dislocation. Since the tectonic deformations in different tectonic belts involved different strata and had different intensities and styles, the oil and gas in different tectonic belts underwent different styles of migration, accumulation, preservation, and destruction (Figure 9) [24,49]. The link in spatial and temporal relationships of the MVT mineralization and hydrocarbon re-accumulation and destruction in the margin of the eastern Sichuan basin, in combination with the ubiquitous presence of high-density methane inclusions, is consistent with, though not necessarily indicative of, the MVT mineralization and hydrocarbon re-accumulation and destruction simultaneously triggered by the Late Jurassic to Early Cretaceous Yanshanian orogeny. We thus propose a model for the local MVT mineralization on and near the sites of former hydrocarbon reservoirs, especially dry gas reservoirs. The Yanshanian compressional tectonics drove a large-scale flow of metal- and sulfate-bearing basinal fluids passed under or through methane-bearing carbonate units. Methane immediately entered the sulfate-bearing solution and began producing hydrogen sulfide by thermochemical sulfate reduction, and then hydrogen sulfide reacted with metal ions to precipitate metal sulfides and release H<sup>+</sup> ions. The CO<sub>2</sub> generated by H<sup>+</sup> ions dissolving the surrounding carbonate rock mixed with the CO<sub>2</sub> generated by the oxidation of methane by thermochemical sulfate reduction, resulting in the supersaturation of CO<sub>2</sub> in the system, and then combined with the Ca<sup>2+</sup>, Mg<sup>2+</sup> ions to precipitate hydrothermal carbonates, while capturing methane inclusions and CH<sub>4</sub>-saturated two-phase aqueous inclusions. The large-scale flow was concentrated in the most permeable rocks, but along faults in some places. The identification of high-density methane inclusions provides evidence for the role of CH<sub>4</sub> as a reducing agent during MVT mineralization.

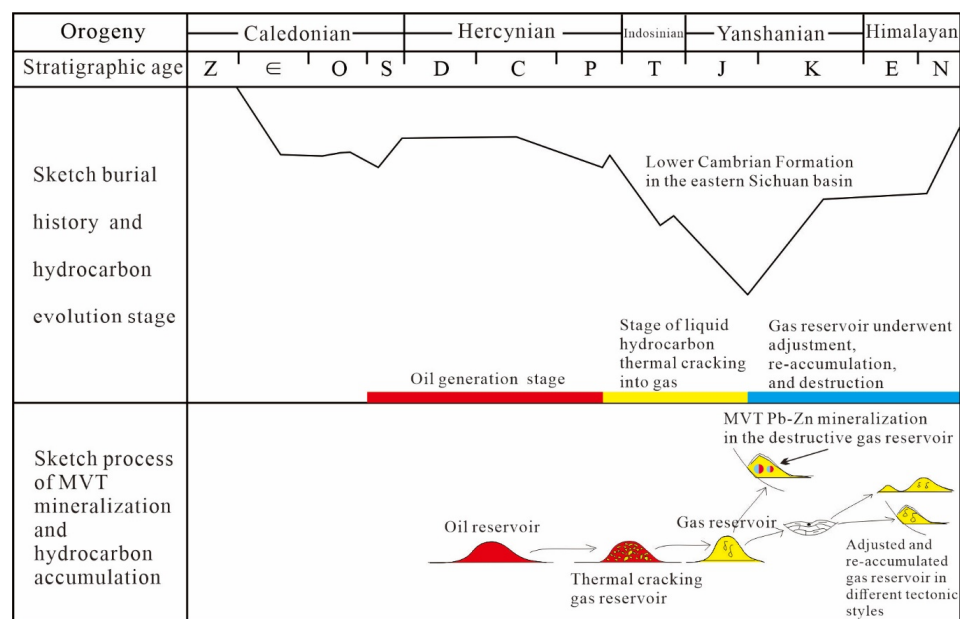


**Figure 9.** Sketch diagram of the ore-forming in the process of hydrocarbon accumulation and destruction in the strong structural deformation area of the eastern Sichuan.

## 6. Conclusions

Based on an integrated investigation of Rb-Sr and Sm-Nd geochronology, Sr isotope geochemistry, and fluid inclusion analysis of MVT Pb-Zn deposits and results from oil and gas accumulation and evolution analyses, the following conclusions can be drawn:

(1) On the basis of the petrography and Raman spectral analyses of fluid inclusions, high-density methane, moderate temperature, and salinity inclusions were discovered in the samples of paragenetic fluorites and calcites from the studied MVT Pb-Zn deposits in the margin of the eastern Sichuan basin. The Raman scatter peak  $\nu_1$  of methane inclusions was applied to calculate the density of methane inclusions. The density of methane inclusions in fluorites from the Wujiahe orebody and calcites from the Laoxi orebody is approximate, mainly ranging from 0.192 g/cm<sup>3</sup> to 0.212 g/cm<sup>3</sup>, 0.210 g/cm<sup>3</sup> to 0.218 g/cm<sup>3</sup>, respectively, which signifies methane inclusions of high density.

(2) Rb-Sr isochron of paragenetic sphalerites and pyrites from the Laochangping Pb-Zn deposit, Sm-Nd isochron of paragenetic fluorites and calcite from the Wujiahe orebody in the Luota Pb-Zn deposit, and Rb-Sr isochron of sphalerites from the Laoxi orebody in the Luota Pb-Zn deposit define isochron ages of 142.9–144.5 Ma, 147.6 Ma, and 138.5 Ma, respectively, indicating that the Late Jurassic to Early Cretaceous was an important metallogenic event in the margin of the eastern Sichuan basin. The <sup>87</sup>Sr/<sup>86</sup>Sr values (0.71088–0.714749) of the MVT Pb-Zn deposits are similar to those of Lower Cambrian Niutitang Formation sources. This, combined with moderate temperature and salinity, and the presence of single-phase high-density methane inclusions, implies that the ore-precipitating fluids could have been derived from the hydrocarbon associated basinal brines rather than from a marine involvement in the fluid source.

(3) The link in spatial and temporal relationships of the MVT mineralization and hydrocarbon accumulation and destruction in the margin of the eastern Sichuan basin, in combination with the ubiquitous presence of high-density methane inclusions, is consistent with, though not necessarily indicative of, the MVT mineralization and hydrocarbon accumulation and destruction simultaneously triggered by the Late Jurassic to the Early Cretaceous Yanshanian orogeny. The identification of high-density methane inclusions provides evidence for the role of CH<sub>4</sub> as a reducing agent during MVT mineralization.

**Author Contributions:** Conceptualization, Z.H. and J.G.; investigation, J.G., S.L. and Z.H.; data curation, S.L.; writing—original draft preparation, J.G.; writing—review and editing, Z.H., J.G., S.L. and S.H.; supervision, S.H.; funding acquisition, Z.H.; All authors have read and agreed to the published version of the manuscript.

**Funding:** This research was jointly funded by the National Natural Science Foundation of China (Nos. U20B6001, U19B6003 and 42002137).

**Data Availability Statement:** Not applicable.

**Acknowledgments:** We thank Jian-xin Zhao, Yue-xing Feng, Jing Xu, and Jia-Qi Yang for their help with analytical work, technical assistance, and constructive comments, which led to substantial improvements in the quality of this article. Our special thanks are extended to the editors and anonymous reviewers for their reviews and constructive suggestions.

**Conflicts of Interest:** The authors declare no conflict of interest.

## References

1. Gize, A.P.; Barnes, H.L. The organic geochemistry of two Mississippi Valley-type lead-zinc deposits. *Econ. Geol.* **1987**, *82*, 457–470. [[CrossRef](#)]
2. Kesler, S.E.; Jones, H.D.; Furman, F.C.; Sassen, R.; Anderson, W.H.; Kyle, J.R. Role of crude oil in the genesis of Mississippi Valley-type deposits: Evidence from the Cincinnati Arch. *Geology* **1994**, *22*, 609–612. [[CrossRef](#)]
3. Wu, Y.; Zhang, C.; Mao, J.; Ouyang, H.; Sun, J. The genetic relationship between hydrocarbon systems and Mississippi Valley-type Zn–Pb deposits along the SW margin of Sichuan Basin, China. *Int. Geol. Rev.* **2013**, *55*, 941–957. [[CrossRef](#)]
4. Gao, J.; Li, Y.; He, S.; He, Z.; Li, S.; Wo, Y.; Li, W.; Zhai, G.; Zhao, J. Exploration Discovery of Shale Gas and Its Indicative Significance to Mineralization of MVT Lead-Zinc Deposit in Yichang Area, West Hubei. *Earth Sci.* **2021**, *46*, 1222–1232, (in Chinese with English abstract).

5. Anderson, G.M. Precipitation of Mississippi Valley-type ores. *Econ. Geol.* **1975**, *70*, 937–942. [[CrossRef](#)]
6. Anderson, G.M. Organic maturation and ore precipitation in Southeast Missouri. *Econ. Geol.* **1991**, *86*, 909–926. [[CrossRef](#)]
7. Cai, C.F.; Worden, R.H.; Bottrell, S.H.; Wang, L.S.; Yang, C.C. Thermochemical sulphate reduction and the generation of hydrogen sulphide and thiols (mercaptans) in Triassic carbonate reservoirs from the Sichuan Basin, China. *Chem. Geol.* **2003**, *202*, 39–57. [[CrossRef](#)]
8. Leach, D.L.; Sangster, D.F.; Kelley, K.D.; Large, R.R.; Garven, G.; Allen, C.R.; Gutzmer, J.; Walters, S. Sediment-Hosted Lead–Zinc Deposits: A Global Perspective. One Hundredth Anniversary Volume; Society of Economic Geologists: Littleton, CO, USA, 2005; pp. 561–608.
9. Zhang, C.Q.; Wu, Y.; Hou, L.; Mao, J.W. Geodynamic setting of mineralization of Mississippi Valley-type deposits in world-class Sichuan–Yunnan–Guizhou Zn–Pb triangle, southwest China: Implications from age-dating studies in the past decade and the Sm–Nd age of Jinshachang deposit. *J. Asian Earth Sci.* **2015**, *103*, 103–114. [[CrossRef](#)]
10. Xiong, S.; Jiang, S.; Ma, Y.; Liu, T.; Zhao, K.; Jiang, M.; Zhao, H. Ore genesis of Kongxigou and Nanmushu Zn–Pb deposits hosted in Neoproterozoic carbonates, Yangtze Block, SW China: Constraints from sulfide chemistry, fluid inclusions, and in situ S–Pb isotope analyses. *Precambrian Res.* **2019**, *333*, 105405. [[CrossRef](#)]
11. Powell, T.G.; Macqueen, R.W. Precipitation of sulfide ores and organic matter sulfate reactions at Pine Point, Canada. *Science* **1984**, *224*, 63–66. [[CrossRef](#)]
12. Xiong, S.; Gong, Y.; Jiang, S.; Zhang, X.; Li, Q.; Zeng, G. Ore genesis of the Wusihe carbonate-hosted Zn–Pb deposit in the Dadu River Valley district, Yangtze Block, SW China: Evidence from ore geology, S–Pb isotopes, and sphalerite Rb–Sr dating. *Miner. Depos.* **2018**, *53*, 967–979. [[CrossRef](#)]
13. Xiong, S.; Jiang, S.; Chen, Z.; Zhao, J.; Ma, Y.; Zhang, D.; Duan, Z.; Niu, P.; Xu, Y. A Mississippi Valley-type Zn–Pb mineralizing system in South China constrained by in situ U–Pb dating of carbonates and barite and in situ S–Sr–Pb isotopes. *Geol. Soc. Am. Bull.* **2022**. [[CrossRef](#)]
14. Xu, J.; Zheng, Y.; Sun, X.; Shen, Y. Alteration and mineralization at the Zhibula Cu skarn deposit, Gangdese belt, Tibet. *Ore Geol. Rev.* **2016**, *75*, 304–326. [[CrossRef](#)]
15. Xu, J.; Zheng, Y.; Sun, X.; Li, X.; Mao, G. Genesis of the Yaguila Pb–Zn–Ag–Mo skarn deposit in Tibet: Insights from geochronology, geochemistry, and fluid inclusions. *J. Asian Earth Sci.* **2019**, *172*, 83–100. [[CrossRef](#)]
16. Rui, Z.Y.; Ye, J.H.; Zhang, L.S.; Mei, Y.X. Pb–Zn Deposits on the Perimeter of the Yangtze Craton and on the Margins of Its Uplifts. *Geol. China* **2004**, *31*, 337–346, (in Chinese with English abstract).
17. Zhou, J.; Huang, Z.; Zhou, M.; Li, X.; Jin, J. Constraints of C–O–S–Pb isotope compositions and Rb–Sr isotopic age on the origin of the Tianqiao carbonate-hosted Pb–Zn deposit, SW China. *Ore Geol. Rev.* **2013**, *53*, 77–92. [[CrossRef](#)]
18. Wang, H.; Ye, L.; Hu, Y.; Wei, C.; Li, Z.; Huang, Z.; Shuang, Y. Trace element characteristics in sphalerites from the Laochangping Pb–Zn deposit in the Southeastern Chongqing. *Acta Mineral. Sin.* **2021**, *41*, 623–634, (in Chinese with English abstract).
19. Li, S.; Li, Y.; He, Z.; Chen, K.; Yan, D. Differential Deformation on Two Sides of Qiyueshan Fault along the Eastern Margin of Sichuan Basin, China, and Its Influence on Shale Gas Preservation. *Mar. Petrol. Geol.* **2020**, *121*, 104602. [[CrossRef](#)]
20. Yan, D.; Bing, Z.; Zhou, M.F.; Wei, G.; Song, H.L.; Liu, S.F. Constraints on the Depth, Geometry and Kinematics of Blind Detachment Faults Provided by Fault-Propagation Folds: An Example from the Mesozoic Fold Belt of South China. *J. Struct. Geol.* **2009**, *31*, 150–162. [[CrossRef](#)]
21. He, Z.L.; Wang, X.; Li, S.; Wo, Y.; Zhou, Y. Yanshan Movement and its influence on petroleum preservation in middle-upper Yangtze region. *Pet. Geol. Exp.* **2011**, *33*, 1–11.
22. Yan, D.; Zhou, M.; Song, H.; Wang, X.; Malpas, J. Origin and tectonic significance of a Mesozoic multi-layer over-thrust system within the Yangtze block (South China). *Tectonophysics* **2003**, *361*, 239–254. [[CrossRef](#)]
23. Fan, Y. *Interrelationship between Tectonism and Hydrocarbon Accumulation in Marine Strata at Critical Tectonic Moment in West Hubei–East Chongqing, South China*; China University of Geosciences: Wuhan, China, 2016; pp. 45–66, (in Chinese with English abstract).
24. Ma, Y.S.; Lou, Z.H.; Guo, T.L.; Fu, X.Y.; Jin, A.M. An Exploration on a Technological System of Petroleum Preservation Evaluation for Marine Strata in South China. *Acta Geol. Sin.* **2006**, *80*, 406–417, (in Chinese with English abstract).
25. Zhang, C.Q. *The Genetic Model of Mississippi Valley-type Deposits in the Boundary Area of Sichuan, Yunnan and Guizhou Province, China*; Chinese Academy of Geological Sciences: Beijing, China, 2008; pp. 1–177, (in Chinese with English abstract).
26. Peng, N.L.; Liang, E.Y.; Liu, W.; Liu, G.Y.; Yuan, F.; Xiong, M.; Huang, L.Q.; Wang, Y.C. A comparative study of Luota Ore Field Lead-zinc Deposits in the Northwest of Hunan Province with Typical MVT Lead-zinc Deposits. *South Met.* **2014**, *04*, 5–16, (in Chinese with English abstract).
27. Goldstein, R.H.; Reynolds, T.J. Systematics of fluid inclusions in diagenetic minerals. SEPM Short Course 31. *Soc. Sediment. Geol.* **1994**, 199. [[CrossRef](#)]
28. Gao, J.; He, S.; Yi, J. Discovery of high density methane inclusions in Jiaoshiba shale gas field and its significance. *Oil Gas Geol.* **2015**, *36*, 472–480, (in Chinese with English abstract).
29. Gao, J.; He, S.; Zhao, J.X.; Yi, J. Geothermometry and geobarometry of overpressured Lower Paleozoic gas shales in the Jiaoshiba field, central China: Insight from fluid inclusions in fracture cements. *Mar. Petrol. Geol.* **2017**, *83*, 124–139. [[CrossRef](#)]
30. Gao, J.; Zhang, J.; He, S.; Zhao, J.; He, Z.; Wo, Y.; Feng, Y.; Li, W. Overpressure generation and evolution in Lower Paleozoic gas shales of the Jiaoshiba region, China: Implications for shale gas accumulation. *Mar. Petrol. Geol.* **2019**, *102*, 844–859. [[CrossRef](#)]

31. Lin, F.; Bodnar, R.; Becker, S. Experimental determination of the Raman CH<sub>4</sub> symmetric stretching ( $\nu_1$ ) band position from 1–650 bar and 0.3–22 °C: Application to fluid inclusion studies. *Geochem. Cosmochim. Acta* **2007**, *71*, 3746–3756. [[CrossRef](#)]
32. Lu, W.; Chou, I.; Burruss, R.; Song, Y. A unified equation for calculating methane vapor pressures in the CH<sub>4</sub>-H<sub>2</sub>O system with measured Raman shifts. *Geochim. Cosmochim. Acta* **2017**, *71*, 3969–3978. [[CrossRef](#)]
33. Wang, Y.X.; Gu, L.X.; Zhang, Z.Z.; Wu, C.Z.; Zhang, K.J.; Li, H.M.; Yang, J.D. Geochronology and Nd–Sr–Pb isotopes of the bimodal volcanic rocks of the Bogda rift. *Acta Petrol. Sin.* **2006**, *22*, 1215–1224, (in Chinese with English abstract).
34. Wopenka, B.; Pasteris, J.D.; Freeman, J.J. Analysis of individual fluid inclusions by Fourier transform infrared and Raman microspectroscopy. *Geochem. Cosmochim. Acta* **1990**, *54*, 519–533. [[CrossRef](#)]
35. Bodnar, R. Revised equation and table for determining the freezing point depression of H<sub>2</sub>O–NaCl solutions. *Geochem. Cosmochim. Acta* **1993**, *57*, 683–684. [[CrossRef](#)]
36. Duan, Z.; Møller, N.; Weare, J.H. An equation of state for the CH<sub>4</sub>-CO<sub>2</sub>-H<sub>2</sub>O system: I. Pure systems from 0 to 1000 °C and 0 to 8000 bar. *Geochim. Cosmochim. Acta* **1992**, *56*, 2605–2617. [[CrossRef](#)]
37. Sallet, R.; Moritz, R.; Fontignie, D. Fluorite <sup>87</sup>Sr/<sup>86</sup>Sr and REE constraints on fluid–melt relations, crystallization time span and bulk D<sup>Sr</sup> of evolved highsilica granites. Tabuleiro granites, Santa Catarina, Brazil. *Chem. Geol.* **2000**, *164*, 81–92. [[CrossRef](#)]
38. Stein, M.; Starinsky, A.; Agnon, A.; Katz, A.; Raab, M.; Spiro, B.; Zak, I. The impact of brine-rock interaction during marine evaporite formation on the isotopic Sr record in the oceans: Evidence from Mt. Sedom, Israel. *Geochem. Cosmochim. Acta* **2000**, *64*, 2039–2053. [[CrossRef](#)]
39. Liu, W.H.; Zhang, X.J.; Zhang, J.; Jiang, M.R. Sphalerite Rb–Sr dating and in situ sulfur isotope analysis of the Daliangzi lead-zinc deposit in Sichuan Province, SW China. *J. Earth. Sci.* **2018**, *29*, 573–586. [[CrossRef](#)]
40. Zindler, A.; Hart, S.R.; Frey, F.A.; Jakobsson, S.P. Nd and Sr isotope ratios and rare earth element abundances in Reykjanes Peninsula basalts evidence for mantle heterogeneity beneath Iceland. *Earth Planet. Sci. Lett.* **1979**, *45*, 249–262. [[CrossRef](#)]
41. Menzies, M.; Murthy, V.R. Nd and Sr isotope geochemistry of hydrous mantle nodules and their host alkali basalts: Implications for local heterogeneities in metasomatically veined mantle. *Earth Planet. Sci. Lett.* **1980**, *46*, 323–334. [[CrossRef](#)]
42. Qi, L.; Zhou, M.F. Platinum-group elemental and Sr–Nd–Os isotopic geochemistry of Permian Emeishan flood basalts in Guizhou Province, SW China. *Chem. Geol.* **2008**, *248*, 83–103. [[CrossRef](#)]
43. Veizer, J.; Ala, D.; Azmy, K.; Bruckschen, P.; Buhl, D.; Bruhn, F.; Carden, G.A.F.; Diener, A.; Ebner, S.; Godderis, Y. <sup>87</sup>Sr/<sup>86</sup>Sr,  $\delta^{13}\text{C}$  and  $\delta^{18}\text{O}$  evolution of Phanerozoic seawater. *Chem. Geol.* **1999**, *161*, 59–88. [[CrossRef](#)]
44. Schneider, J.; Boni, M.; Lapponi, F.; Bechstädt, T. Carbonate-Hosted Zinc-Lead Deposits in the Lower Cambrian of Hunan, South China: A Radiogenic (Pb, Sr) Isotope Study. *Econ. Geol.* **2002**, *97*, 1815–1827. [[CrossRef](#)]
45. Sawaki, Y.; Ohno, T.; Tahata, M.; Komiya, T.; Hirata, T.; Maruyama, S.; Windley, B.; Han, J.; Shu, D.; Lie, Y. The Ediacaran Radiogenic Sr Isotope Excursion in the Doushantuo Formation in the Three Gorges Area, South China. *Precambrian Res.* **2010**, *176*, 46–64. [[CrossRef](#)]
46. Hu, R.; Wang, W.; Li, S.Q.; Yang, Y.Z.; Chen, F.K. Sedimentary Environment of Ediacaran Sequences of South China: Trace Element and Sr–Nd Isotope Constraints. *J. Geol.* **2016**, *124*, 769–789. [[CrossRef](#)]
47. Liu, J.M.; Zhan, S.R.; Shen, J.; Jiang, N.; Huo, W.G. Review on direct isotopic dating of hydrothermal ore-forming processes. *Prog. Geophys.* **1998**, *13*, 46–55, (in Chinese with English abstract).
48. Jin, Z.J.; Yuan, Y.S.; Liu, Q.Y.; Wo, Y.J. Controls of Late Jurassic–Early Cretaceous Tectonic Event on Source Rocks and Seals in Marine Sequences, South China. *Sci. China Earth Sci.* **2012**, *42*(12), 1791–1801. [[CrossRef](#)]
49. He, Z.L.; Li, S.J.; Wo, Y.J.; Zhang, D.W.; Gu, Y.; Zhou, Y. Major Factors Controlling Hydrocarbon Preservation Condition in the Marine Basins of China and its Evaluation Ideas. *Acta Petrol. Sin.* **2017**, *33*, 1222–1232, (in Chinese with English abstract).